PNAS
www.pnas.org

Supplementary Information for

Structural Basis for Antiarrhythmic Drug Interactions with the Human Cardiac Sodium Channel

Phuong T. Nguyen[1,3], Kevin R. DeMarco[1,3], Igor Vorobyov[1,2], Colleen E. Clancy[1,2*], Vladimir Yarov-Yarovoy[1*]

[1]Department of Physiology and Membrane Biology, University of California Davis, Davis, United States;
[2]Department of Pharmacology, University of California Davis, Davis, United States;
[3]Biophysics Graduate Group, University of California Davis, Davis, United States

*For correspondence:
ceclancy@ucdavis.edu (CEC)
yarovoy@ucdavis.edu (VY-Y)

This PDF file includes:

Other supplementary materials for this manuscript include the following:

Supplementary Information Text

www.pnas.org/cgi/doi/10.1073/pnas.1817446116

SI Results and Discussion

hNav1.5 channel residues forming the putative antiarrhythmic and local anesthetic drug binding site

Key amino acid residues forming the putative antiarrhythmic and local anesthetic drug binding site in DIIIS6 and DIVS6 segments (1-4) are identical between hNa$_V$1.5 and eeNa$_V$1.4 (SI Appendix, Fig. S2). For example, F1760 and Y1767 in the DIVS6 segment in hNa$_V$1.5 (Fig. 1A) are F1555 and Y1562 in eeNa$_V$1.4, respectively. Moreover, L1462 and I1466 in the DIIIS6 segment in hNa$_V$1.5 (Fig. 1A) are L1256 and I1260 in eeNa$_V$1.4, respectively.

hNav1.5 channel residues forming the drug access pathway at the fenestration between the DIIIS6 and DIVS6

I1756 in the DIVS6 segment in hNa$_V$1.5 is also identical in eeNa$_V$1.4 (I1551) and forms part of the drug access pathway at the fenestration between the DIIIS6 and DIVS6 segments (see SI Appendix, Fig. S2) (2). However, another key amino acid residue in the drug access pathway at the fenestration between DIIIS6 and DIVS6 segments (5) is different between hNa$_V$1.5 and eeNa$_V$1.4: T1753 in the DIVS6 segment of hNa$_V$1.5 is C1548 in eeNa$_V$1.4 (see Fig. 1B, SI Appendix, Figs. S2 and S3). Notably, T1753 is facing L1413 in the P1-helix of DIII, which is a unique residue in the fenestration between the DIIIS6 and DIVS6 segments because all other Na$_V$ channel domains have a Phenylalanine at the corresponding position (see SI Appendix, Figs. S3 and S4).

Modeling of antiarrhythmic and local anesthetic drugs interaction with human Na$_V$1.5 channel using RosettaLigand.

QX-314 is a permanently charged derivative of lidocaine with a quaternary ammonium group. The most frequently sampled lowest binding energy RosettaLigand models of QX-314 interacting with hNav1.5 indicate that the region above F1760 in the DIVS6 segment forms a "hot spot" for QX-314 binding (Fig. 2C and SI Appendix, Fig. S7), which is similar to the "hot spot" observed in our lidocaine – hNav1.5 models. The ammonium group of QX-314 is positioned above F1760 (Fig. 2C). The phenyl ring of QX-314 is observed in multiple different orientations near F1760 (Fig. 2C and SI Appendix, Fig. S7).

Etidocaine is a local anesthetic drug that was used in the first experimental study by the Catterall group that identified key residues of the receptor site for state-dependent block in both the DIVS6 segment (F1760 and Y1767 in hNa$_V$1.5) (2) and the DIIIS6 segment (L1462 and I1466 in hNa$_V$1.5) (4). The most frequently sampled lowest binding energy RosettaLigand models of charged etidocaine show the molecule binding above F1760 in the DIVS6 segment (Fig. 2D and SI Appendix, Fig. S8), which is similar to the "hot spot" observed in our lidocaine and QX-314 – hNav1.5 models. The ammonium group of etidocaine is positioned above and near F1760 (Fig. 2D). The phenyl ring of etidocaine is observed in multiple different orientations near F1760 (Fig. 2D and SI Appendix, Fig. S8).

Neutral and charged lidocaine partitioning into the membrane

The molecular docking calculations provided us with atomistic structural models of convergent binding poses of several anti-arrhythmic and local anesthetic drugs in the hNa$_V$1.5 pore (see Figs. 2 and 3). However, static molecular models cannot tell us how a drug accesses the binding site and whether such drug - protein interactions are long-lived or transient. Such information can be provided by atomistic molecular dynamics (MD) simulations of a channel embedded in a hydrated lipid membrane with one or multiple drug molecules present. To perform such simulations, we need accurate atomic-resolution structural models, called empirical force fields, for all the system components. For this study, we used biomolecular and generalized all-atom CHARMM force fields as described in SI Appendix and SI Methods.

We focused the MD simulations on hNav1.5 interactions with charged and neutral forms of lidocaine. This widely used antiarrhythmic and local anesthetic drug was chosen for our exploratory MD study because molecular docking calculations and previous experimental data indicate that it shares the same binding site as larger Na$_V$1.5 blockers such as flecainide and ranolazine. Our previous MD simulation study of drug – bacterial Nav channel interactions suggested that we can more efficiently predict entry and egress pathways for a smaller drug, like the local anesthetic benzocaine, compared to the larger anti-epileptic drug phenytoin (6). Indeed, experimental data indicate that lidocaine has faster Na$_V$1.5 association and dissociation kinetics than the larger flecainide (7). Moreover, in aqueous solution lidocaine exists as a mixture with a substantial fractions of both charged (~78% at pH=7.4) and neutral form (~22% at pH=7.4) which have different membrane permeabilities and can interact with the ion channels via distinct pathways, as was discussed above. Previous experimental and simulation studies suggested that charged and neutral forms of lidocaine differently affect Na$_V$ channel function (7-9). Therefore, in this study we have explored charged and neutral lidocaine – lipid membrane and Na$_V$1.5 interactions via all-atom MD simulations. We developed force field parameters for charged and neutral lidocaine, because they are not available in the standard biomolecular (10, 11) or generalized CHARMM force field (CGENFF) (12). We used gas-phase quantum mechanical (QM) drug geometries, vibrational frequencies, dihedral angle profiles, dipole magnitude and direction as well as interactions with water in different orientations as reference values for the parameter development, as described in SI Appendix SA1 and illustrated in SI Appendix, Figs. S11 and S12 and Tables S1-S3.

Lidocaine free energy profiles, used to obtain our log$D$ estimate using Eq. 2 below are shown in SI Appendix, Fig. S13 and demonstrate that there is a higher barrier for charged vs. neutral lidocaine translocation across a lipid membrane in agreement with a previous study using different drug models (8). However, contrary to ~5 kcal/mol free energy well at the membrane center for neutral lidocaine in that study (8), our simulations predict an interfacial minimum of -1.09 kcal/mol at $|z|$ = 13 Å and a ~4.64 kcal/mol peak at the membrane center (SI Appendix, Fig. S13). We also obtained even more favorable interfacial binding of –3.07 kcal/mol at $|z|$ = 15 Å for charged lidocaine, which despite a larger peak of 6.58 kcal/mol at the membrane center leads to a more favorable membrane partitioning of this form. The partitioning coefficients for neutral and charged lidocaine forms computed using Eq. (1) below, were logK_0 = 0.12 +/- 0.40 and logK_1 = 1.35 +/- 0.14 respectively. Experimentally, logK_0 has been measured to be in the range of 2.1 to 2.39

(13), while logK_I has been measured in the range 0.9 to 1.49 (13) depending on the experimental conditions. The distribution coefficient log D = 1.25 ± 0.32 computed using Eq. (2) below was fairly consistent with experimental values of 1.4 (14) and 1.76 (13), despite an underestimated partition coefficient for the neutral form of the drug since the charged form is dominant at physiological pH. We also used an approximation of Kramer's transition rate theory to estimate the transition rates (15, 16) of charged and neutral forms of lidocaine through a simulated POPC bilayer. We used the same approach as in our previous study (17) and for charged and neutral lidocaine computed their diffusion coefficients (18) close to the membrane center using Hummer's method, as well as the curvatures around the binding wells and peaks (i.e. free energy minima and maxima) , estimated from second derivatives of second-order polynomial fits to the relevant portion of each respective free energy profile. Estimated transition rates through the membrane are 38.9 s^{-1} for charged lidocaine and 21.1ms^{-1} for the neutral drug form, indicating three orders of magnitude faster crossing rate for the latter.

Since charged lidocaine is the dominant drug form at a physiological pH 7.4 (~78.4% based on its pK_a = 7.96) (14), we primarily expect the accumulation of charged drug at water-membrane interfaces, in agreement with recent solid NMR experiments (19). However, deeper into the hydrophobic membrane core, neutral lidocaine is expected to be the more dominant form and should be able to translocate across a membrane more easily due to the substantially smaller barrier than its protonated counterpart (~6 kcal/mol vs. ~10 kcal/mol) (SI Appendix, Fig. S13). This indicates that we need to study both charged and neutral lidocaine interactions with hNa$_V$1.5 to assess hydrophobic (lipid-mediated access through channel fenestrations) and hydrophilic (water-mediated access through an intracellular gate) channel pore drug access pathways and understand molecular mechanisms of channel activity modulation.

SI Methods

Rosetta modeling of the hNa$_V$1.5 channel

We used the Rosetta structural modeling software (20-22) and the cryoEM structure of the Na$_V$1.4-beta1 complex from the electric eel (eeNa$_V$1.4) (PDB ID: 5XSY) as a template to predict the structure of the human Na$_V$1.5 (hNa$_V$1.5) channel. At first, the structure of eeNa$_V$1.4 without the beta1 subunit was passed through the Cryo-EM refinement protocol in Rosetta (23). The lowest scoring density-refitted eeNa$_V$1.4 model and electron density were then used in combination in RosettaCM (24) to model the hNa$_V$1.5 channel. We generated 5,000 structural models of hNa$_V$1.5 and selected the top 500 lowest-scoring models for clustering analysis as described previously (25). Models from top clusters were visually inspected to select the final model for the docking study.

RosettaLigand modeling of hNa$_V$1.5 channel interaction with antiarrhythmic and local anesthetic drugs

OpenEye OMEGA (OpenEye Scientific Software) (26, 27) was used to generate conformers for antiarrhythmic and local anesthetic drugs. To uniformly and efficiently sample the pore region of hNa$_V$1.5, drugs were placed at 5 different initial locations: at the center of the cavity and at 4 fenestration sites. We incorporated an initial random perturbation with a translation distance less than 10 Å before the docking run to add another layer of randomization. Sampling radius was set to 10 Å. The details of the RosettaLigand

docking algorithm have been described previously (20, 28-31) (see Rosetta scripts and command lines used in Appendix SA1). A total of 200,000 docking models were generated for each drug. The top 10,000 models were selected based on the total score of protein-ligand complex and then ranked by ligand binding energy represented by Rosetta interface delta_X energy term. The top 50 ligand binding energy models were visually analyzed using UCSF Chimera (32) and the most frequently sampled ensembles of poses are shown in Figures 2 and 3, with several representative poses demonstrated in Figure 2 and 3 Figure Supplements.

Drug forcefield parameterization

We obtained the molecular structure of lidocaine from the ZINC database (accession number 20237), (33), and used the CGENFF program, version 1.0 (34, 35) to generate initial guesses for partial atomic charges, bond lengths, bond angles, and dihedral angles.

The initial topology and parameters for charged and neutral forms lidocaine were subsequently validated and optimized using QM target data following the suggested CGENFF force field methodology (36). High-quality parameters not already present in CGENFF are assigned from existing parameters based on chemical analogy, and our optimizations focused on parameters with poor chemical analogy corresponding to a high penalty score (35). The Force Field Toolkit plugin (ffTK) (37) for the Visual Molecular Dynamics program (VMD) (38) was used to generate files for quantum mechanical (QM) reference calculations and to perform parameter optimizations. QM target data for parameter optimization were obtained utilizing Møller–Plesset (MP2) and Hartree-Fock (HF) electronic structure methods and the 6-31(d) basis set using the Gaussian 09 program (39).

MP2/6-31G(d) molecular dipole magnitude and orientation as well as scaled HF/6-31G(d) interaction energies with water were used for the optimization of partial atomic charges compatible with the CHARMM atomistic force fields (40). Internal bond and angle parameters were validated by comparison to MP2/6-31G(d) optimized geometries and scaled vibrational frequencies, and differences within 0.01 Å and 1° between QM and MM equilibrium bond and angle values were sought. Finally, the dihedral angle parameters were optimized to reproduce MP2/6-31G(d) potential energy scans for rotation around a particular bond.

Optimized charges (Table S1) are in good agreement with QM target dipole values. The optimized MM dipole moments are overestimated in magnitude from QM MP2/6-31G(d) dipole moments by 17% for neutral lidocaine and 16% for charged lidocaine (close to a 20% acceptable lower-end threshold, suggested for the CGENFF force field), and the MM dipole direction differed by ~1° from the QM computed direction for both charged and neutral lidocaine. The water interaction distances were all within 0.4 Å of QM target values (see Tables S2 and S3). The MM dipole moment for charged lidocaine (11.7 Debye) is ~3 times higher than for neutral lidocaine (3.9 Debye), which agrees with respective computed QM values. Water interaction energies were also in good agreement with QM values, with root mean squared errors (RMSE) of 0.95 kcal/mol for neutral lidocaine, and 1.41 kcal/mol for charged lidocaine, respectively (Table S4). For neutral lidocaine, there was a high penalty score for the C2-N1-C3 bond angle, and optimization yielded a difference of 0.16° between MM and QM values. For charged lidocaine there were no high penalties for

internal bond and angle parameters from the CGENFF. For neutral lidocaine, there were four high-penalty dihedral angles, and for charged lidocaine there were two high-penalty dihedral angles from the CGENFF. Dihedral optimizations resulted in great improvement over CGENFF initial guesses (illustrated SI Appendix, Figs. S11 and S12), with optimized torsional energy minima within ~2 kcal/mol of QM values. For comparison, raw CGENFF dihedral parameters with high penalties yielded QM free energy minima differences sometimes as high ~5kcal/mol.

Final topology and parameters for neutral and charged lidocaine are provided in the Appendix SA2.

Drug-membrane partitioning

Partitioning of charged and neutral lidocaine into a lipid membrane was assessed using the NAMD (41) program. Initial system setup scripts were generated with the CHARMM-GUI web toolkit (42) and were modified to build the hydrated drug-membrane systems, which consisted of 128 1-palmitoyl-2-oleoylphosphatidylcholine (POPC) lipids, ~7000 water molecules, 21 or 22 K^+ and 22 Cl^- ions to ensure 0.15 M electrolyte concentration and overall electrical neutrality, and one drug molecule, totaling ~38,250 atoms. CHARMM36 lipid force field (10), TIP3P water model (43), standard CHARMM ion parameters (44) and CGENFF (12) compatible drug parameters developed in this work were used throughout all simulations.

For partitioning calculations of each drug we used the umbrella sampling (US) method (45) with 81 independent simulation windows, placing the center of mass (COM) of a randomly oriented drug molecule in 1 Å intervals from -40 Å to 40 Å with respect to COM of the membrane. The COM of the drug was restrained along the *z* axis with a force constant of 2.5 kcal/mol/Å^2, and an additional 5 kcal/mol/Å^2 cylindrical restraint was applied in order to prevent the drift of the molecule in the *xy* plane. Each NAMD US simulation of charged and neutral lidocaine was carried out in a *NPT* ensemble with 1 atm pressure maintained by Langevin piston barostat (46), and 310K, controlled by Nosé-Hoover thermostat (47, 48). Tetragonal cells with periodic boundary conditions (PBC) were used in all the simulations, and the SHAKE algorithm (49) was employed to fix the bonds to all hydrogen atoms, allowing for the use of a 2 fs time step. Electrostatic interactions were computed via Particle Mesh Ewald (50), with a mesh grid of 1 Å.

Potential of mean force (PMF) profiles were computed using the weighted histogram analysis method (WHAM) (51). Umbrella sampling simulations for charged and neutral lidocaine were run for 15 ns per window. Standard errors in PMFs were computed as a measure of asymmetries with respect to the membrane center (z=0).

Drug-water partition coefficients were calculated as was done previously (52):

$$K(\text{wat}\rightarrow\text{mem}) = \frac{1}{(z_2 - z_1)} \int_{z_1}^{z_2} e^{-\frac{\{W(z) - W(z_1)\}}{k_B T}} dz \qquad (1)$$

where $W(z)$ is the PMF, z_1 and z_2 are points in aqueous solution on opposite sides of the membrane, k_B is Boltzmann constant, and T is the absolute temperature.

The distribution coefficient, log D, was computed as

$$\log D = \log(K_0 + K_1 10^{pKa-pH}) - \log(1 + 10^{pKa-pH}) \quad (2)$$

where K_0 is the partition coefficient of a neutral drug form, and K_1 is the partition coefficient of a charged (protonated) drug form (13). Standard errors for log K and log D were estimated from asymmetries in free energy profiles via propagation of uncertainties.

To compute drug translocation rates across membrane we used Kramer's transition rate approximation as was done previously (15, 16). For charged lidocaine local diffusion near the membrane center was computed to be $D(z_{barrier})$=0.0047 Å^2/ps, and the curvatures of the PMF well and the PMF peak were 0.0508 and -0.207, respectively. For neutral lidocaine $D(z_{barrier})$=0.0089 Å^2/ps, and the curvatures of the PMF well and the PMF peak were 0.0312 and -0.0784, respectively.

Molecular dynamics simulations of hNa$_V$1.5 channel interaction with lidocaine

The hNa$_V$1.5 model was embedded in a bilayer of POPC with explicit TIP3P water molecules and 150 mM (with lidocaine) or 500 mM (without lidocaine) of NaCl using CHARMM-GUI (53). For lidocaine containing simulations we used physiological NaCl concentration, but we used larger salt concentration in the drug-free runs to facilitate Na^+ conductance. For all these simulations, we also used CHARMM36 lipid (54) and protein (11) force fields, and CHARMM generalized force field (CGENFF) compatible parameters for lidocaine as described above. Initial system equilibrations were performed using NAMD on a local GPU cluster. After 10,000 steps of steepest descent minimization, MD simulations started with a timestep of 1 fs with harmonic restraints initially applied to protein heavy atoms and some lipid tail dihedral angles. These restraints were slowly released over 2 ns. Harmonic restraints (0.1 kcal/mol/Å^2) were then applied only to protein C_α atoms, and the systems were equilibrated further for 50 ns with a timestep of 2 fs. In order to use a 2 fs timestep, all bonds to H atoms were constrained using the SHAKE algorithm. All simulations were performed at constant pressure (1 atm) with constant ratio of x and y dimensions in order to maintain the correct area per lipid, and constant temperature of 303.15 K (chosen to avoid the gel phase transition of POPC lipids). Electrostatic interactions were computed using Particle Mesh Ewald (PME). Non-bonded pair lists were updated every 10 steps with a list cutoff distance of 16 Å and a real space cutoff of 12 Å with energy switching starting at 10 Å.

Equilibrated systems were simulated on the Anton 2 supercomputer using Anton 2 software (55) version 1.31.0 in the *NPT* ensemble at 303.15 K. A 2 fs timestep was used with non-bonded long-range interactions computed every 6 fs using the RESPA multiple time step algorithm. The multi-integrator (multigrator) algorithm was used for temperature and semi-isotropic pressure coupling. Long-range electrostatic interactions were handled by u-series algorithm (55). A long-range Lennard-Jones (LJ) correction (beyond cutoff) was not used as was suggested for CHARMM36 lipid force field. For the simulation of hNa$_V$1.5 without

drugs, an electric field was applied downwardly in the *z* direction to mimic membrane potential of 250 mV (positive inside).

For the neutral lidocaine simulations, two different systems were created with initial neutral lidocaine aqueous concentration at 75mM and 150mM. Each system was simulated for 7 μs on Anton2.

For the charged lidocaine simulations, systems of 1 and 2 charged lidocaine were created by initially placing 1 and 2 charged lidocaine molecules in the cavity of the hNav1.5 model. Each system was simulated for 1 μs on Anton2.

Analysis

Drug binding in the channel: 3D density maps of the drug center of mass for the neutral lidocaine and position of the amino group for the charged one from $Na_V1.5$ – drug flooding MD simulations were used to compute free energy profiles using equation $W(r_i) = -k_BTln[\rho(r_i)] + C$ where $\rho(r_i)$ is the unbiased probability distribution as a function of reaction coordinates r_i, and C is a constant. The maps were offset to get an average free energy of 0 kcal/mol in bulk water for neutral lidocaine or for the binding site in the pore for the charged lidocaine. 2D projections of these free energy maps on the *Z* (transmembrane) and *Y* (lateral) axes are shown in Figs. 4, 5 and 6. Origin is selected as the center of mass of the protein.

Sodium binding in the selectivity filter (Fig. 7): xy-radial position ≤ 15Å, and z-axial position between -15 and +15 Å were used to define the pore region for ion occupation. x, y and z are defined relative to the center of mass (COM) of the backbone of the selectivity filter. Free energy surfaces were calculated from unbiased simulation as $W(r_i) = -k_BTln[\rho(r_i)] + C$ where $\rho(r_i)$ is the unbiased probability distribution as a function of reaction coordinates r_i, and C is a constant. Origin is selected as the center of mass of the protein.


hNav1.5
eeNav1.4
DI-S1
DI-S2
DI-S3
DI-S4
DI-S5
DI-P1
DI-P2
DI-S6
DII-S1
DII-S2
DII-S3
DII-S4
DII-S5
DII-P1
DII-P2
DII-S6
DIII-S1
DIII-S2
DIII-S3
DIII-S4

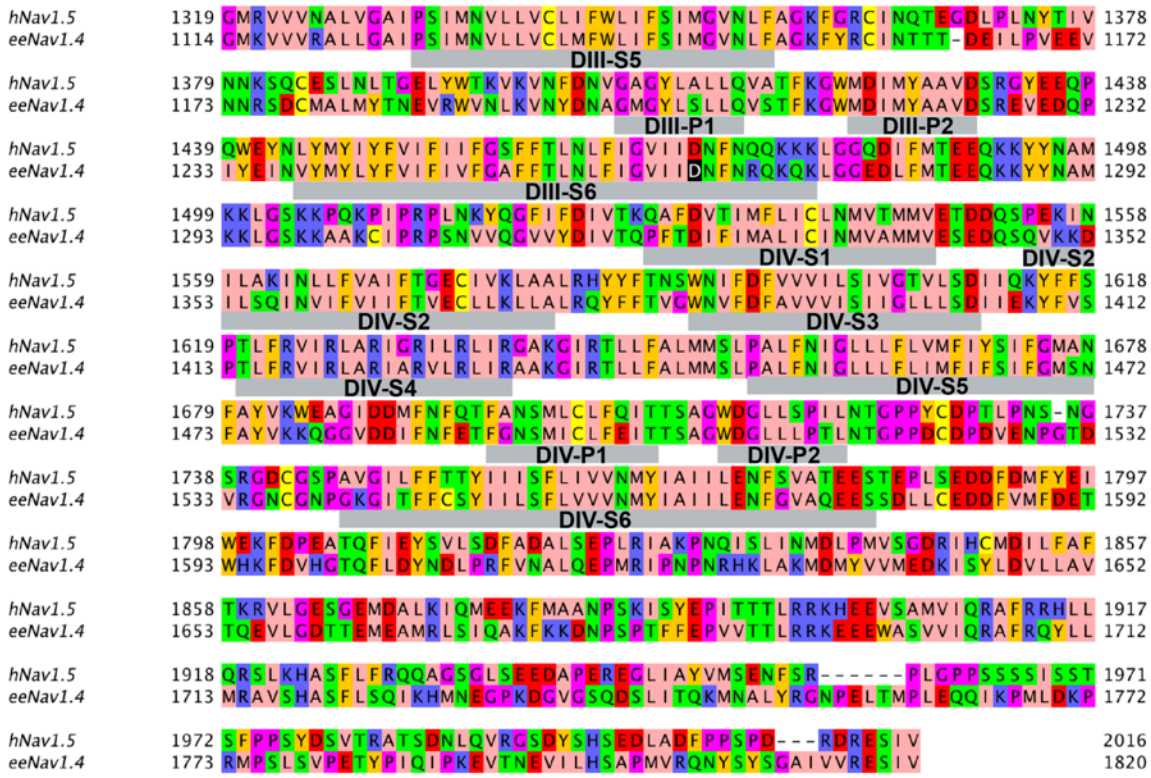

Fig. S1. Sequence alignment between hNav1.5 and eeNav1.4. Transmembrane segments S1-S6 and P1 and P2 helix regions in each domain are underlined by gray bars and labeled. Amino acids were colored with Jalview program using the Zappo color scheme, where hydrophobic residues (I, L, V, A, and M) are colored pink, aromatic residues (F, W, and Y) are colored orange, positively charged residues (K, R, and H) are colored blue, negatively charged residues (D and E) are colored red, hydrophilic residues (S, T, N, and Q) are colored green, P and G colored magenta, and C is colored yellow.

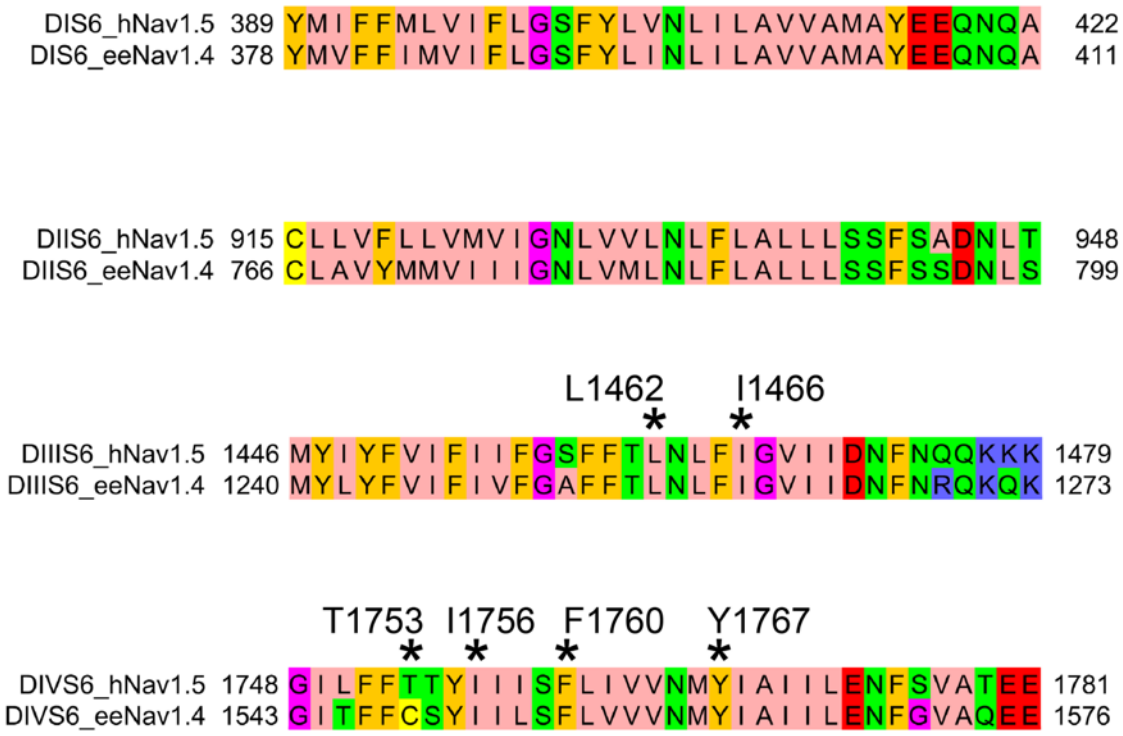

Fig. S2. Sequence alignment between hNav1.5 and eeNav1.4 transmembrane segments S6. Specific hNav1.5 residues discussed in the main text are marked by asterisk and labeled. Amino acids were colored as in Fig. S1.

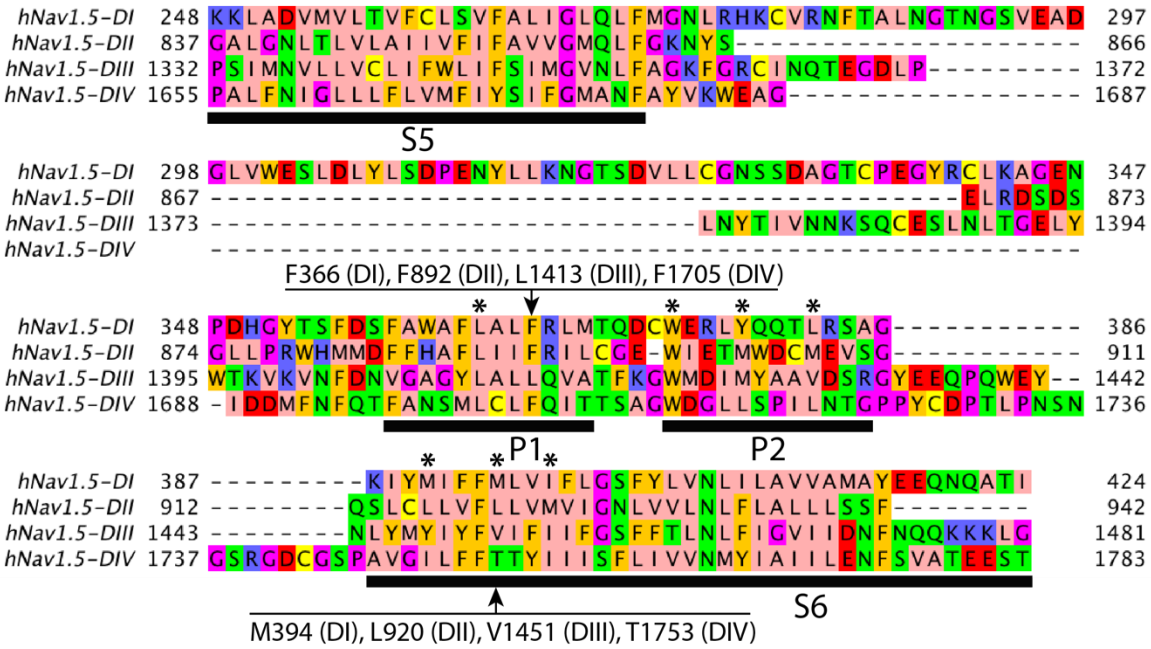

Fig. S3. Sequence alignment between four domains of hNav1.5 segments S5, P1-helix, P2-helix, and S6. Specific hNav1.5 residues discussed in the main text are marked by arrows and labeled. Residues facing the lipid environment at the interface between the P1-helix from domain III and P2-helix and S6 segment from domain IV are marked by asterisks. Transmembrane segments S5 and S6 and P1 and P2 helix regions in each domain are underlined by black bars and labeled. Amino acids were colored as in Fig. S1.

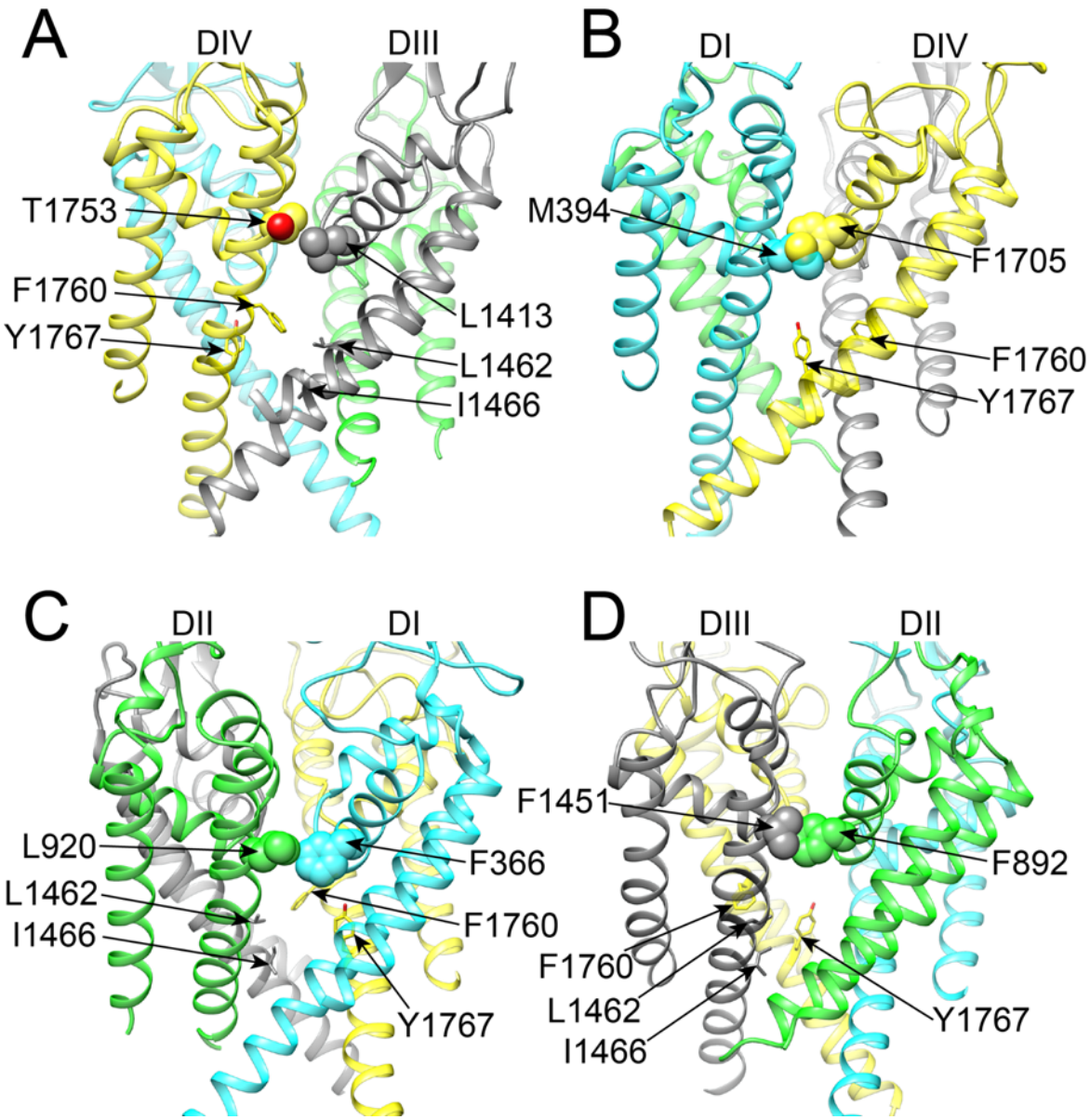

Fig. S4. Transmembrane views of all four hNav1.5 fenestrations. (A) DIII and DIV fenestration. (B) DI and DIV fenestration. (C) DI and DII fenestration. (D) DII and DIII fenestration. Side chains of fenestration-forming residues are shown in space-filling or stick representations, labeled, and colored using corresponding domain colors, with O atom shown in red.

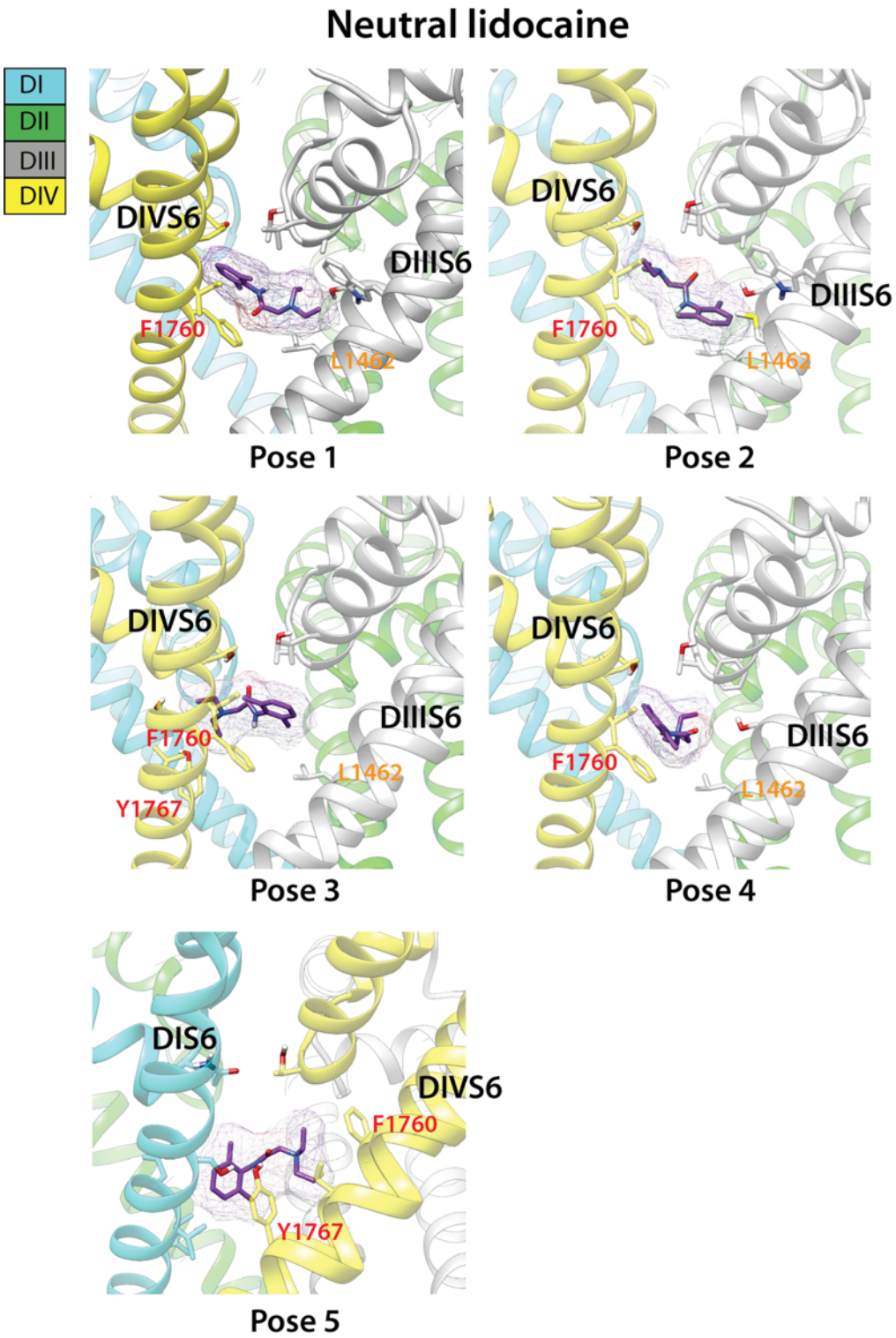

Fig. S5. Top binding poses of neutral lidocaine interaction with Rosetta model of hNav1.5 channel. Domain I is colored in blue, domain II is colored in green, domain III is colored gray, and domain IV is colored yellow. hNav1.5 residues forming interactions with lidocaine are shown in stick representation and labeled. Lidocaine is shown in stick and surface representation and colored purple.

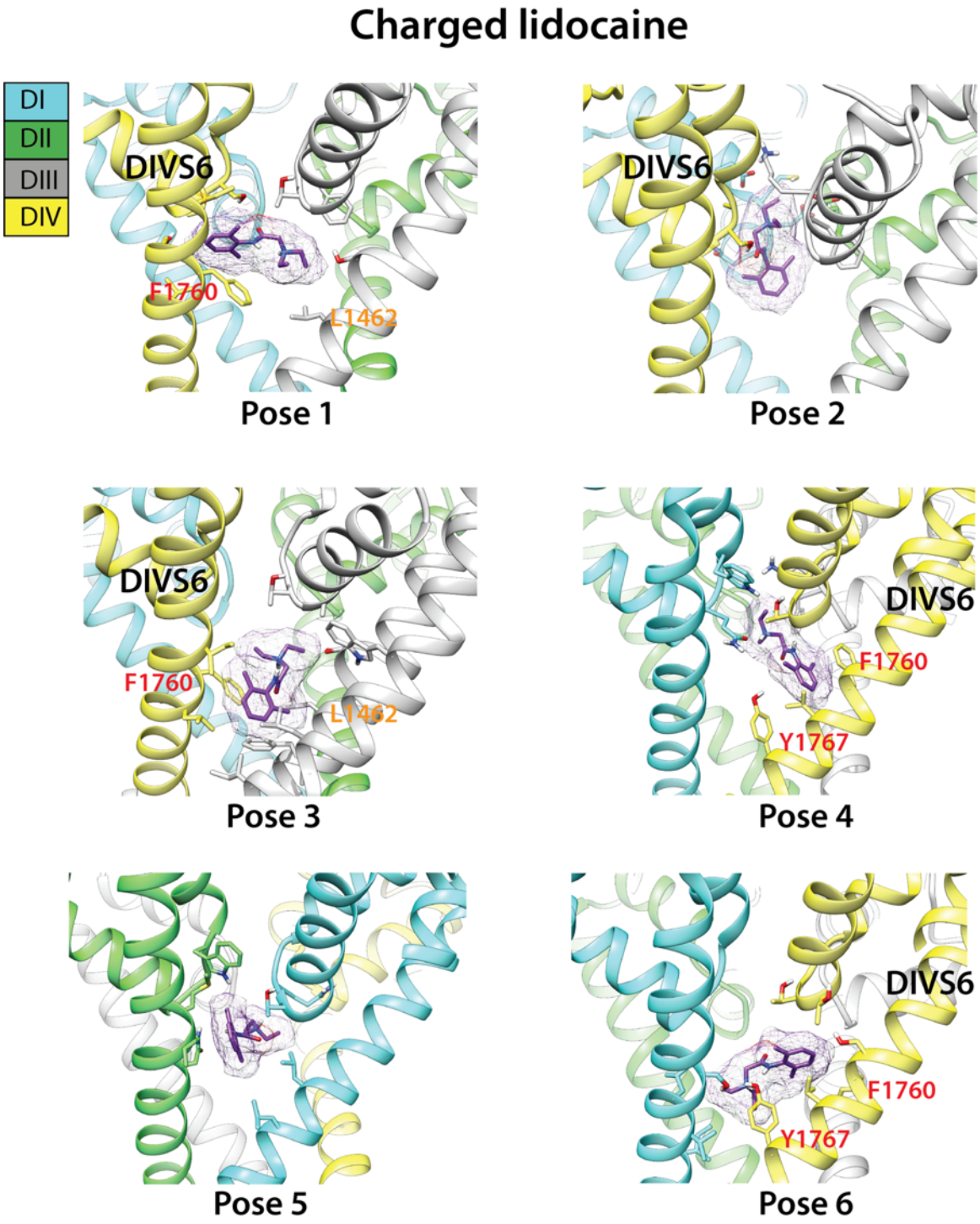

Fig. S6. Top binding poses of charged lidocaine interaction with Rosetta model of hNav1.5 channel. Domain I is colored in blue, domain II is colored in green, domain III is colored gray, and domain IV is colored yellow. hNav1.5 residues forming interactions with lidocaine are shown in stick representation and labeled. Lidocaine is shown in stick and surface representation and colored purple.

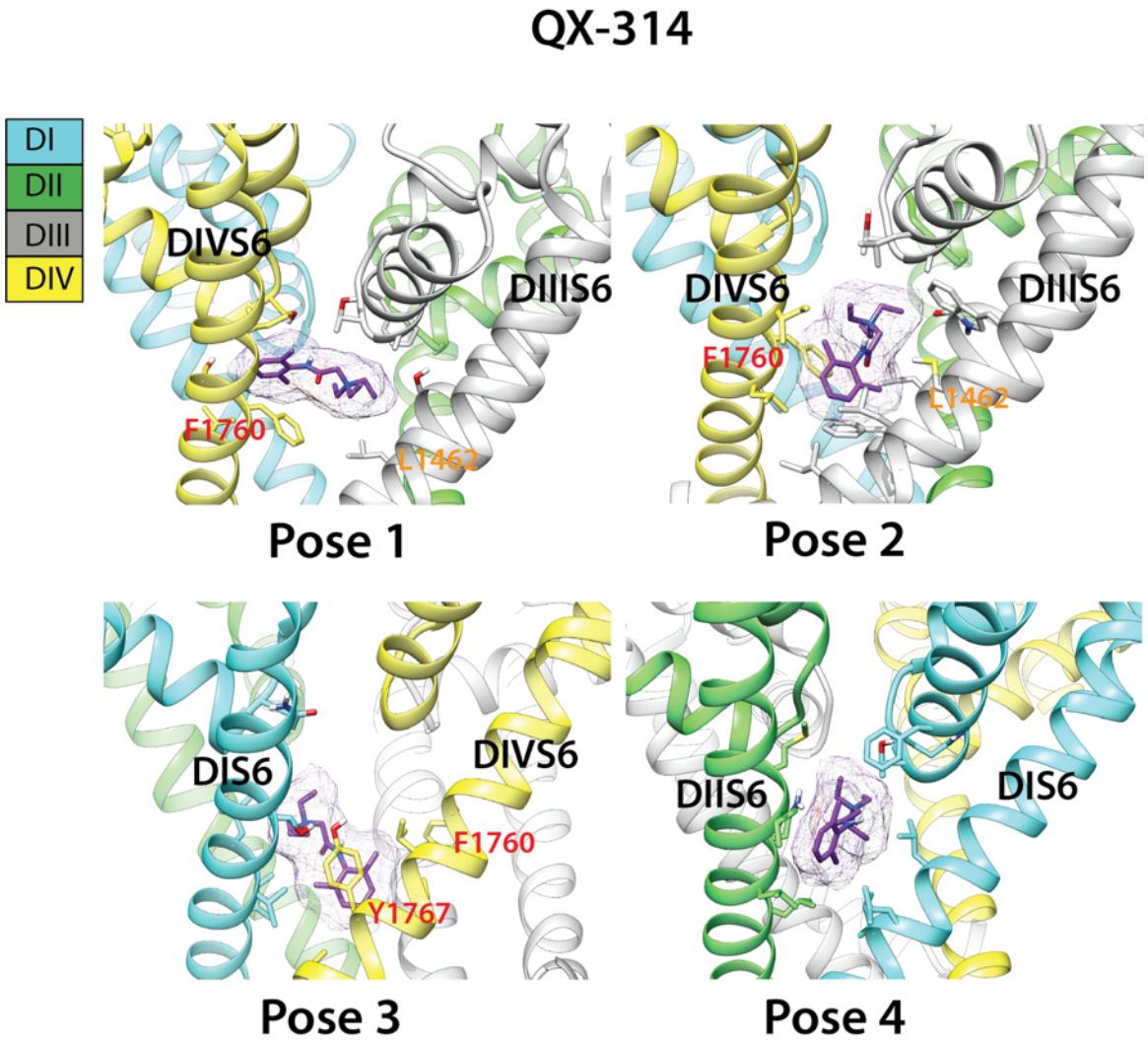

Fig. S7. Top binding poses of QX-314 interaction with Rosetta model of hNav1.5 channel. Domain I is colored in blue, domain II is colored in green, domain III is colored gray, and domain IV is colored yellow. hNav1.5 residues forming interactions with lidocaine are shown in stick representation and labeled. QX-314 is shown in stick and surface representation and colored purple.

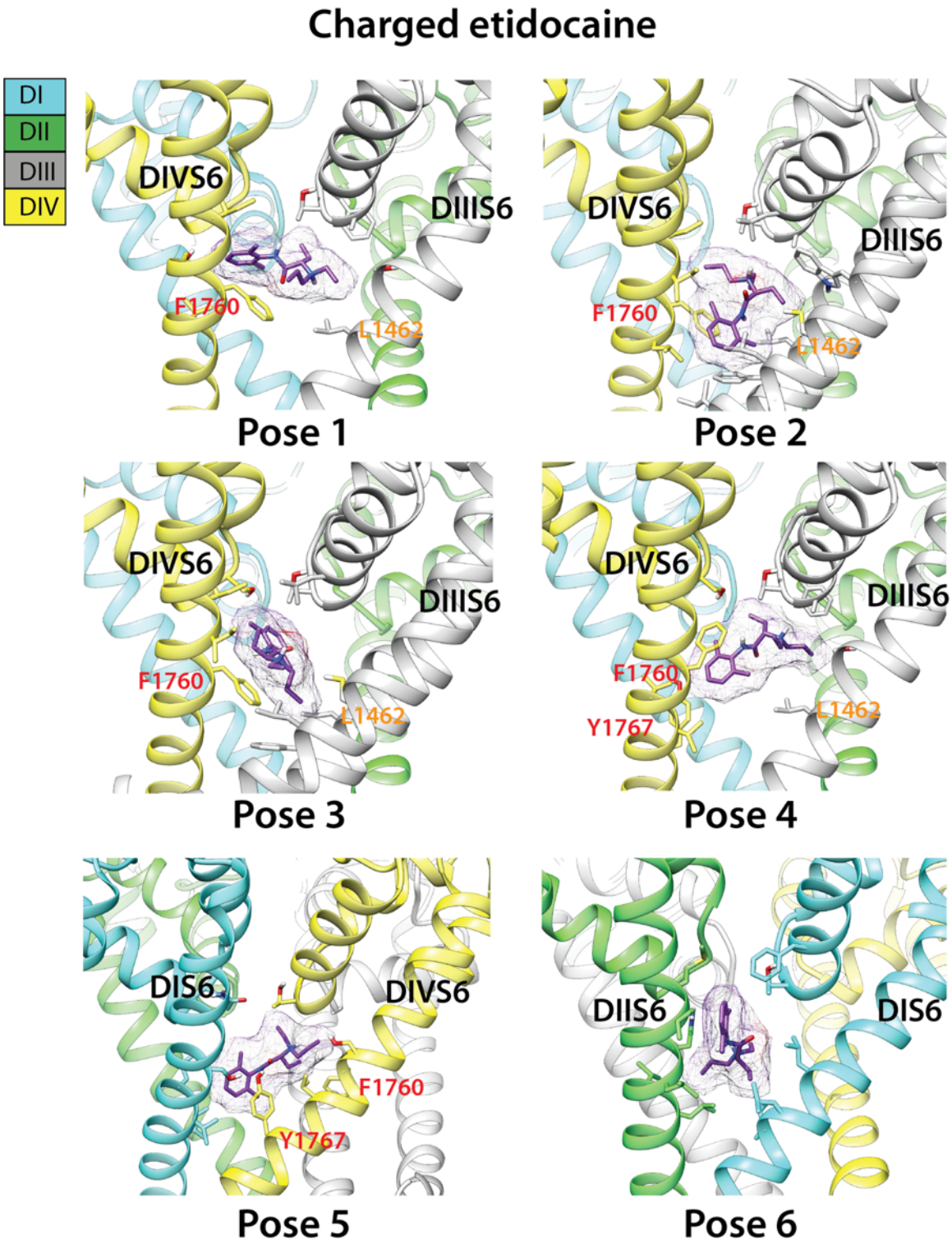

Fig. S8. Top binding poses of charged etidocaine interaction with Rosetta model of hNav1.5 channel. Domain I is colored in blue, domain II is colored in green, domain III is colored gray, and domain IV is colored yellow. hNav1.5 residues forming interactions with lidocaine are shown in stick representation and labeled. Etidocaine is shown in stick and surface representation and colored purple.

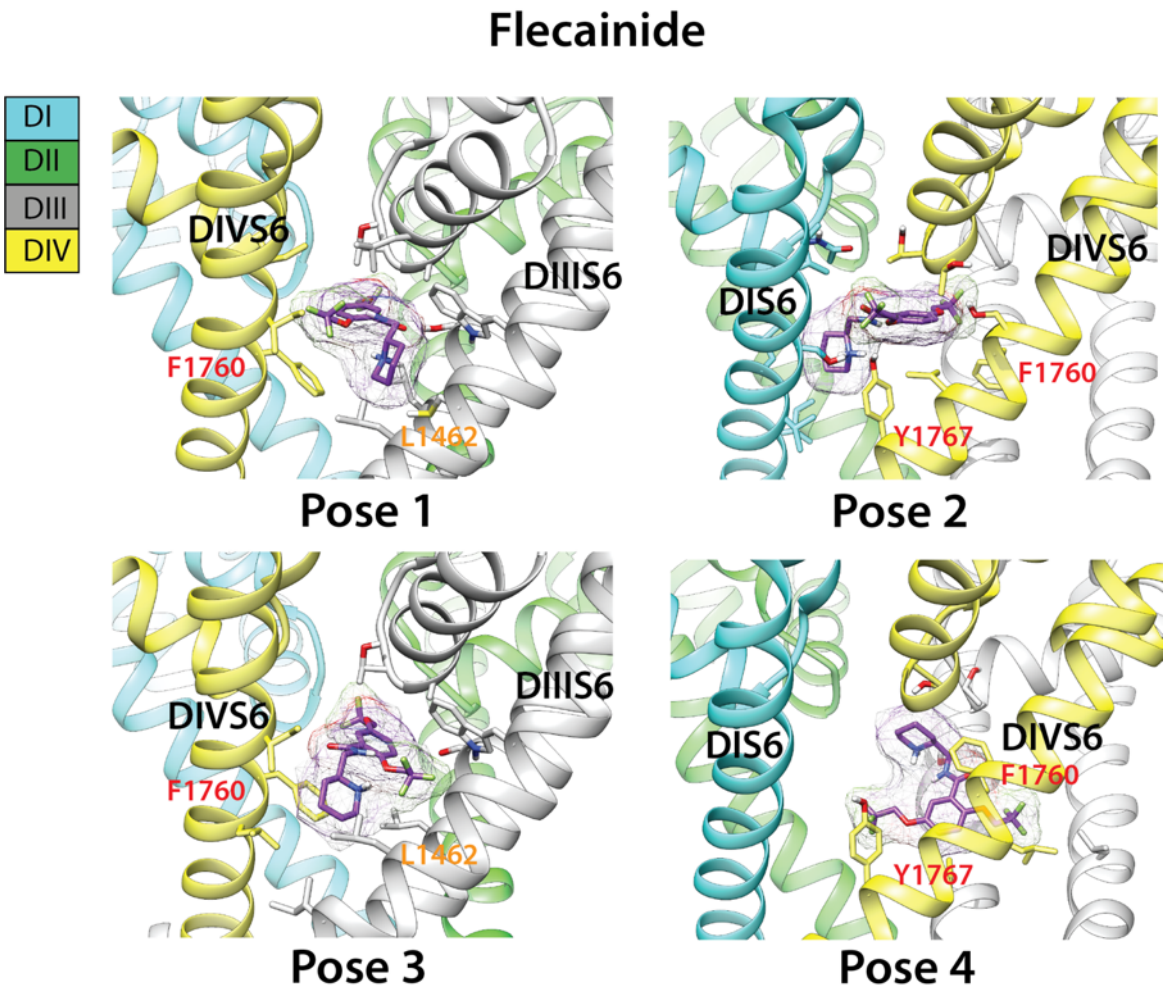

Fig. S9. Top binding poses of flecainide interaction with Rosetta model of hNav1.5 channel. Domain I is colored in blue, domain II is colored in green, domain III is colored gray, and domain IV is colored yellow. hNav1.5 residues forming interactions with lidocaine are shown in stick representation and labeled. Flecainide is shown in stick and surface representation and colored purple.

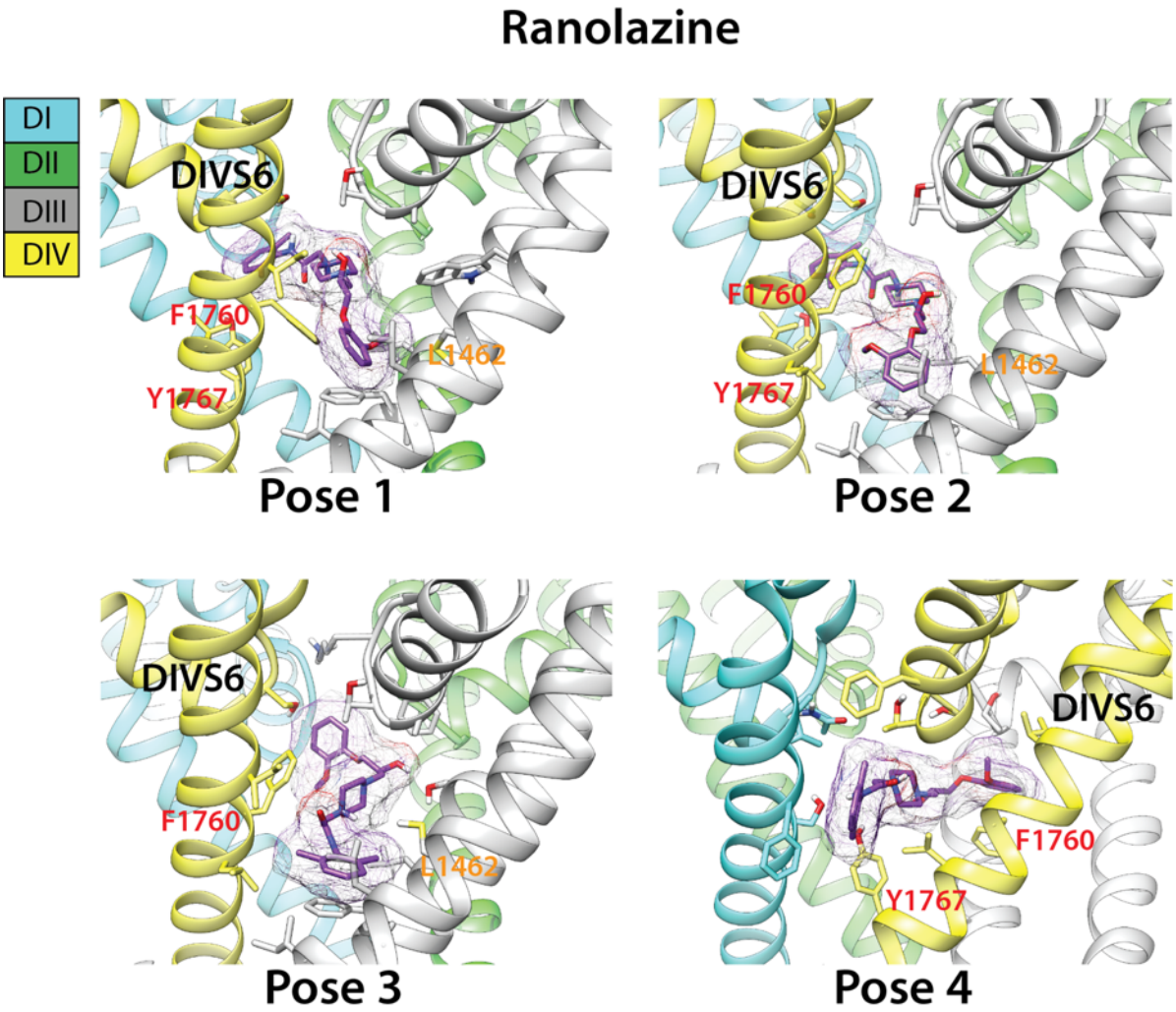

Fig. S10. Top binding poses of ranolazine interaction with Rosetta model of hNav1.5 channel. Domain I is colored in blue, domain II is colored in green, domain III is colored gray, and domain IV is colored yellow. hNav1.5 residues forming interactions with lidocaine are shown in stick representation and labeled. Ranolazine is shown in stick and surface representation and colored purple.

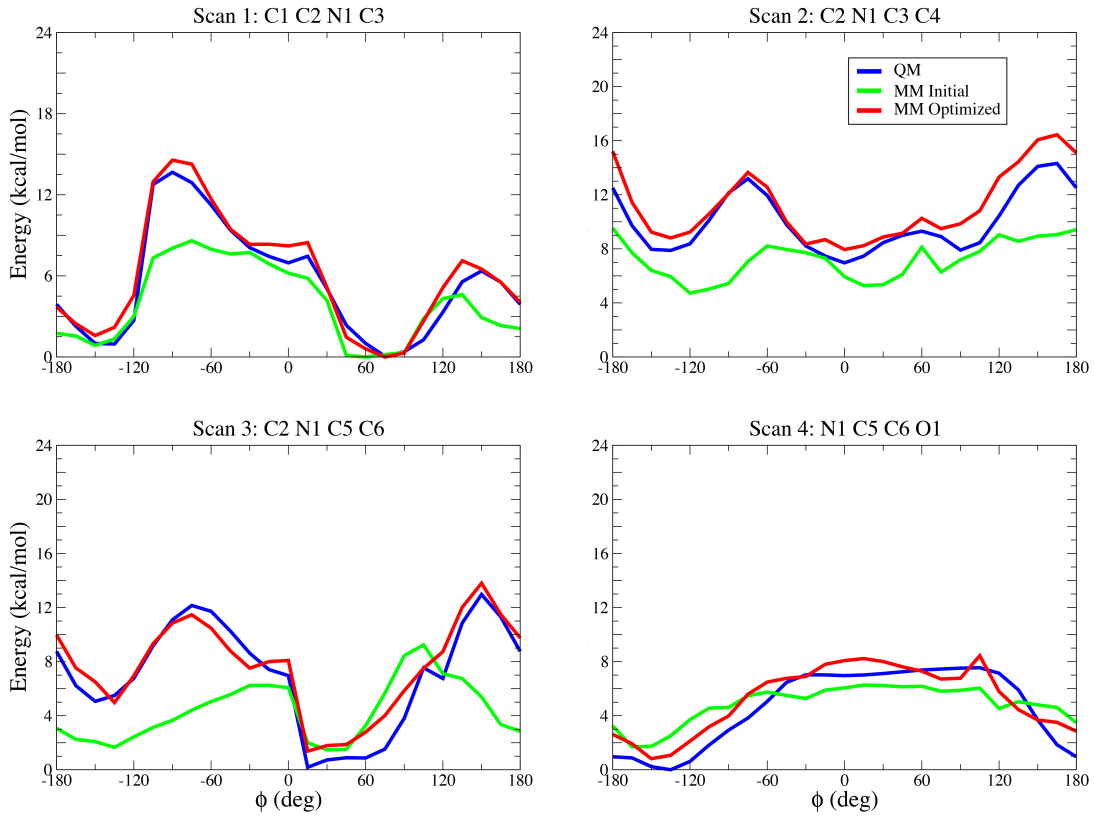

Fig. S11. Gas-phase torsional energy profiles for neutral lidocaine (LID0) from quantum mechanical (QM), initial and optimized molecular mechanics (MM) calculations. Atom names correspond to ones in topology and parameter files.

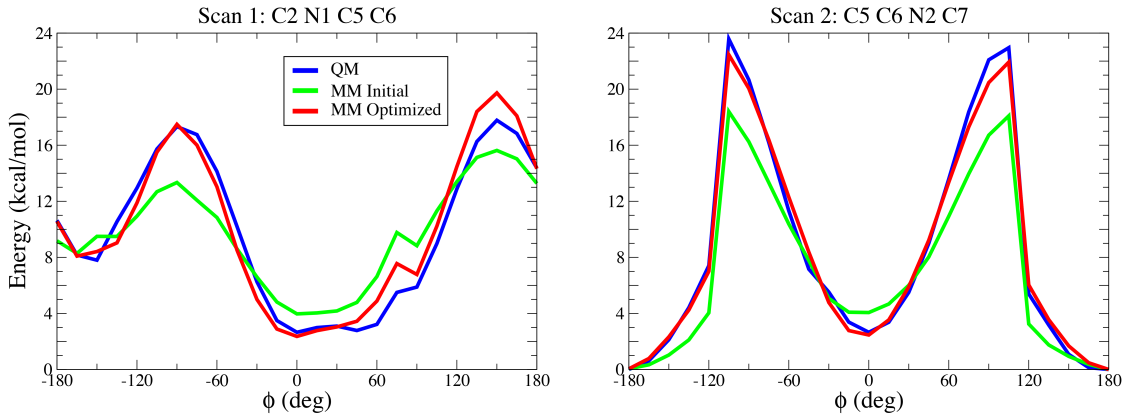

Fig. S12. Gas-phase torsional energy profiles for charged lidocaine (LID1) from quantum mechanical (QM), initial and optimized molecular mechanics (MM) calculations. Atom names correspond to ones in topology and parameter files.

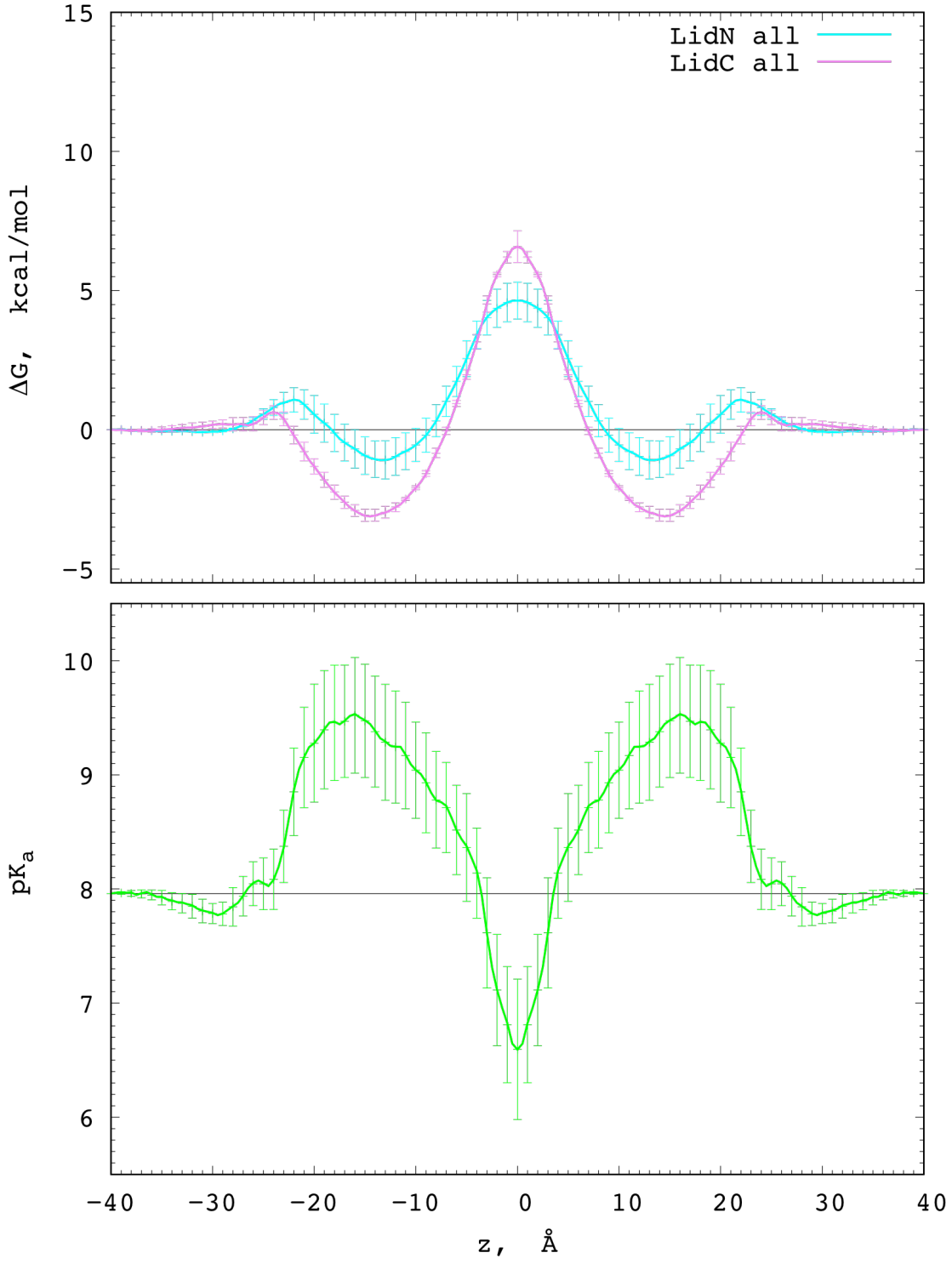

Fig. S13. Charged and neutral lidocaine translocation across a POPC membrane. PMF profiles for POPC membrane crossing neutral (cyan) and charged (magenta) drug (top) and corresponding pKa profile (bottom). Error bars computed as a measure of asymmetry.

Table S1. Partial atomic charges for charged (LID1) and neutral (LID0) lidocaine models. Optimized charge values are shown by asterisk.

	LID1		LID0
C1	-0.268	C1	-0.273
C2 *	0.057	C2	-0.048
N1 *	-0.264	N1 *	-0.515
C3 *	0.057	C3	-0.048
C4	-0.268	C4	-0.273
C5 *	0.493	C5 *	0.31
C6 *	0.101	C6 *	0.635
O1	-0.372	O1	-0.491
N2 *	-0.393	N2 *	-0.749
C7 *	0.021	C7 *	0.477
C8 *	0.249	C8 *	0.409
C9	-0.11	C9	-0.11
C10	-0.113	C10	-0.113
C11	-0.11	C11	-0.11
C12*	0.249	C12*	0.409
C13*	-0.466	C13*	-0.897
C14*	-0.466	C14*	-0.897
H1	0.09	H1	0.09
H2	0.09	H2	0.09
H3	0.09	H3	0.09
H4	0.09	H4	0.09
H5	0.09	H5	0.09
H6	0.09	H6	0.09
H7	0.09	H7	0.09
H8	0.09	H8	0.09
H9	0.09	H9	0.09
H10	0.09	H10	0.09
H11	0.09	H11	0.09
H12	0.09	H12	0.09
H13	0.318	H13	0.319
H14	0.115	H14	0.115
H15	0.115	H15	0.115
H16	0.115	H16	0.115
H17	0.09	H17	0.09
H18	0.09	H18	0.09
H19	0.09	H19	0.09
H20	0.09	H20	0.09
H21	0.09	H21	0.09
H22	0.09	H22	0.09
H23	0.32		

Table S2. Gas-phase cationic lidocaine (LID1) – water interactions.

LID0						
	QME	MME	MME-QME	QMD	MMD	MMD-QMD
N1	-9.401	-8.017	1.384	3.115	3.115	0
N2	-0.265	-1.823	-1.558	5.664	5.264	-0.4
O1	-6.963	-6.138	0.825	2.96	2.96	0
H1	-0.452	-0.369	0.083	2.902	3.002	0.1
H2	-1.196	-0.46	0.736	2.84	3.04	0.2
H3	0.074	0.781	0.707	2.529	2.879	0.35
H4	-0.735	-1.274	-0.539	2.958	2.908	-0.05
H6	-1.222	-0.693	0.529	3.099	3.399	0.3
H7	-1.166	-1.891	-0.725	2.904	2.904	0
H8	-0.983	-0.83	0.153	2.836	2.936	0.1
H9	-2.948	-3.704	-0.756	2.866	2.966	0.1
H10	-0.8	-0.241	0.559	2.706	2.956	0.25
H11	-2.826	-2.991	-0.165	3.017	3.167	0.15
H12	-1.855	-3.259	-1.404	2.659	2.759	0.1
H13	-6.193	-6.374	-0.181	2.225	2.175	-0.05
H14	-1.864	-1.331	0.533	2.578	2.878	0.3
H15	-1.517	-1.633	-0.116	2.614	2.864	0.25
H16	-1.59	-1.096	0.494	2.586	2.886	0.3
H17	1.485	1.99	0.505	2.958	3.358	0.4
H18	-1.188	0.222	1.41	2.73	3.13	0.4
H19	-1.394	-1.066	0.328	3.116	3.516	0.4
H20	-2.655	-1.013	1.642	2.588	2.988	0.4
H21	-1.946	-0.159	1.787	2.634	3.034	0.4
H22	-4.707	-2.995	1.712	2.423	2.823	0.4
RMSE			**0.95**			**0.27**

Table S3. Gas-phase neutral lidocaine (LID0) – water interactions.

LID1						
	QME	MME	MME-QME	QMD	MMD	MMD-QMD
N2	0.88	0.56	-0.33	6.28	5.88	-0.40
O1	-4.00	-5.78	-1.78	3.01	2.91	-0.10
H1	-6.39	-4.80	1.60	2.37	2.77	0.40
H2	-8.40	-6.33	2.06	2.44	2.79	0.35
H3	-7.64	-5.686	1.95	2.271	2.67	0.4
H4	-9.043	-8.254	0.79	2.304	2.70	0.4
H6	-8.438	-6.531	1.91	2.753	3.15	0.4
H7	-9.138	-8.449	0.69	2.301	2.70	0.4
H8	-6.663	-4.984	1.68	2.361	2.76	0.4
H9	-8.891	-7.261	1.63	2.447	2.80	0.35
H10	-7.672	-5.898	1.77	2.323	2.72	0.4
H11	-9.779	-8.519	1.26	2.573	2.97	0.4
H12	-11.085	-10.402	0.68	2.208	2.61	0.4
H13	-13.116	-13.253	-0.14	2.013	2.06	0.05
H14	-4.7	-2.893	1.81	2.417	2.82	0.4
H15	-4.274	-2.576	1.70	2.416	2.82	0.4
H16	-4.453	-2.732	1.72	2.433	2.83	0.4
H17	-4.021	-2.87	1.15	4.599	5.00	0.4
H18	-4.503	-2.996	1.51	2.514	2.86	0.35
H19	-5.583	-5.227	0.36	3.086	3.44	0.35
H20	-5.584	-4.465	1.12	2.533	2.83	0.3
H21	-4.857	-3.112	1.75	2.479	2.83	0.35
H22	-4.789	-3.724	1.07	2.7	3.00	0.3
H23	-3.948	-3.501	0.45	3.194	3.54	0.35
RMSE			**1.41**			**0.36**

Movie S1. Molecular dynamics simulation of hNav1.5 channel interaction with lidocaine reveals hydrophilic drug access pathway. Transmembrane view of hNav1.5 channel model (colored in light gray) with sidechains of F1760 and Y1767 shown in stick representation. Lidocaine molecule that accessed the pore lumen through the intracellular gate is shown in spacefilling representation and colored in cyan with nitrogen atoms colored in blue and oxygen atom colored in red. The pore-forming domains I and IV are shown in the front view during the first half of the movie. The pore-forming domains III and IV are shown in the front view during the second half of the movie.

Movie S2. Molecular dynamics simulation of hNav1.5 channel interaction with lidocaine reveals hydrophobic and hydrophilic drug access pathways. Transmembrane view of hNav1.5 channel model (colored in light gray) with sidechains of F1760 and Y1767 shown in stick representation. Lidocaine molecule that accessed the pore lumen through the fenestration between domains III and IV is shown in spacefilling representation and colored in cyan with nitrogen atoms colored in blue and oxygen atom colored in red. Lidocaine molecule that accessed the pore lumen through the intracellular gate is shown in spacefilling representation and colored in purple. Side chains of residues that form hydrophobic access pathway for lidocaine are shown in stick representation and colored in dark gray. The pore-forming domains III and IV are shown in the front view during most of the movie. The pore-forming domains I and IV are shown in the front view at the end of the movie.

Supplementary References

1. Ragsdale DS, McPhee JC, Scheuer T, & Catterall WA (1996) Common molecular determinants of local anesthetic, antiarrhythmic, and anticonvulsant block of voltage-gated Na+ channels. *Proc Natl Acad Sci U S A* 93(17):9270-9275.
2. Ragsdale DS, McPhee JC, Scheuer T, & Catterall WA (1994) Molecular determinants of state-dependent block of Na+ channels by local anesthetics. *Science* 265(5179):1724-1728.
3. Yarov-Yarovoy V*, et al.* (2002) Role of amino acid residues in transmembrane segments IS6 and IIS6 of the Na+ channel alpha subunit in voltage-dependent gating and drug block. *J Biol Chem* 277(38):35393-35401.
4. Yarov-Yarovoy V*, et al.* (2001) Molecular determinants of voltage-dependent gating and binding of pore-blocking drugs in transmembrane segment IIIS6 of the Na(+) channel alpha subunit. *J Biol Chem* 276(1):20-27.
5. Qu Y, Rogers J, Tanada T, Scheuer T, & Catterall WA (1995) Molecular determinants of drug access to the receptor site for antiarrhythmic drugs in the cardiac Na+ channel. *Proc Natl Acad Sci U S A* 92(25):11839-11843.
6. Boiteux C*, et al.* (2014) Local anesthetic and antiepileptic drug access and binding to a bacterial voltage-gated sodium channel. *Proc Natl Acad Sci U S A*.
7. Moreno JD*, et al.* (2011) A computational model to predict the effects of class I anti-arrhythmic drugs on ventricular rhythms. *Sci Transl Med* 3(98):98ra83.
8. Buyan A, Sun D, & Corry B (2018) Protonation state of inhibitors determines interaction sites within voltage-gated sodium channels. *Proc Natl Acad Sci U S A*.
9. Tikhonov DB & Zhorov BS (2017) Mechanism of sodium channel block by local anesthetics, antiarrhythmics, and anticonvulsants. *J Gen Physiol* 149(4):465-481.
10. Klauda JB*, et al.* (2010) Update of the CHARMM all-atom additive force field for lipids: validation on six lipid types. *J Phys Chem B* 114(23):7830-7843.
11. Huang J & MacKerell AD, Jr. (2013) CHARMM36 all-atom additive protein force field: validation based on comparison to NMR data. *J Comput Chem* 34(25):2135-2145.
12. Vanommeslaeghe K*, et al.* (2010) CHARMM general force field: A force field for drug-like molecules compatible with the CHARMM all-atom additive biological force fields. *J Comput Chem* 31(4):671-690.
13. Avdeef A, Box KJ, Comer JE, Hibbert C, & Tam KY (1998) pH-metric logP 10. Determination of liposomal membrane-water partition coefficients of ionizable drugs. *Pharm Res* 15(2):209-215.
14. Pless SA, Galpin JD, Frankel A, & Ahern CA (2011) Molecular basis for class Ib anti-arrhythmic inhibition of cardiac sodium channels. *Nat Commun* 2:351.
15. Allen TW, Andersen OS, & Roux B (2003) Structure of gramicidin a in a lipid bilayer environment determined using molecular dynamics simulations and solid-state NMR data. *J Am Chem Soc* 125(32):9868-9877.
16. Crouzy S, Woolf TB, & Roux B (1994) A molecular dynamics study of gating in dioxolane-linked gramicidin A channels. *Biophys J* 67(4):1370-1386.
17. DeMarco KR, Bekker S, Clancy CE, Noskov SY, & Vorobyov I (2018) Digging into Lipid Membrane Permeation for Cardiac Ion Channel Blocker d-Sotalol with All-Atom Simulations. *Front Pharmacol* 9:26.

18. Hummer G (2005) Position-dependent diffusion coefficients and free energies from Bayesian analysis of equilibrium and replica molecular dynamics simulations. *New Journal of Physics* 7:34-34.
19. Weizenmann N, Huster D, & Scheidt HA (2012) Interaction of local anesthetics with lipid bilayers investigated by (1)H MAS NMR spectroscopy. *Biochim Biophys Acta* 1818(12):3010-3018.
20. Bender BJ*, et al.* (2016) Protocols for Molecular Modeling with Rosetta3 and RosettaScripts. *Biochemistry* 55(34):4748-4763.
21. Alford RF*, et al.* (2017) The Rosetta All-Atom Energy Function for Macromolecular Modeling and Design. *J Chem Theory Comput* 13(6):3031-3048.
22. Rohl CA, Strauss CE, Misura KM, & Baker D (2004) Protein structure prediction using Rosetta. *Methods Enzymol* 383:66-93.
23. DiMaio F*, et al.* (2015) Atomic-accuracy models from 4.5-A cryo-electron microscopy data with density-guided iterative local refinement. *Nat Methods* 12(4):361-365.
24. Song Y*, et al.* (2013) High-resolution comparative modeling with RosettaCM. *Structure* 21(10):1735-1742.
25. Bonneau R*, et al.* (2002) De novo prediction of three-dimensional structures for major protein families. *J Mol Biol* 322(1):65-78.
26. Hawkins PC & Nicholls A (2012) Conformer generation with OMEGA: learning from the data set and the analysis of failures. *J Chem Inf Model* 52(11):2919-2936.
27. Hawkins PC, Skillman AG, Warren GL, Ellingson BA, & Stahl MT (2010) Conformer generation with OMEGA: algorithm and validation using high quality structures from the Protein Databank and Cambridge Structural Database. *J Chem Inf Model* 50(4):572-584.
28. Combs SA*, et al.* (2013) Small-molecule ligand docking into comparative models with Rosetta. *Nat Protoc* 8(7):1277-1298.
29. DeLuca S, Khar K, & Meiler J (2015) Fully Flexible Docking of Medium Sized Ligand Libraries with RosettaLigand. *PLoS One* 10(7):e0132508.
30. Meiler J & Baker D (2006) ROSETTALIGAND: protein-small molecule docking with full side-chain flexibility. *Proteins* 65(3):538-548.
31. Davis IW & Baker D (2009) RosettaLigand docking with full ligand and receptor flexibility. *J Mol Biol* 385(2):381-392.
32. Pettersen EF*, et al.* (2004) UCSF Chimera--a visualization system for exploratory research and analysis. *J Comput Chem* 25(13):1605-1612.
33. Irwin JJ & Shoichet BK (2005) ZINC--a free database of commercially available compounds for virtual screening. *Journal of chemical information and modeling* 45(1):177-182.
34. Vanommeslaeghe K & MacKerell AD (2012) Automation of the CHARMM General Force Field (CGenFF) I: Bond Perception and Atom Typing. *Journal of chemical information and modeling* 52(12):3144-3154.
35. Vanommeslaeghe K, Raman EP, & MacKerell AD (2012) Automation of the CHARMM General Force Field (CGenFF) II: Assignment of Bonded Parameters and Partial Atomic Charges. *Journal of chemical information and modeling* 52(12):3155-3168.

36. Vanommeslaeghe K*, et al.* (2010) CHARMM General Force Field: A Force Field for Drug-Like Molecules Compatible with the CHARMM All-Atom Additive Biological Force Fields. *J. Comput. Chem.* 31(4):671-690.
37. Mayne CG, Saam J, Schulten K, Tajkhorshid E, & Gumbart JC (2013) Rapid parameterization of small molecules using the Force Field Toolkit. *J Comput Chem* 34(32):2757-2770.
38. Humphrey W, Dalke A, & Schulten K (1996) VMD: visual molecular dynamics. *J Mol Graph* 14(1):33-38, 27-38.
39. Frisch M*, et al.* (2009) Gaussian 09. Wallingford, CT: Gaussian. (Inc).
40. Mackerell AD, Jr. (2004) Empirical force fields for biological macromolecules: overview and issues. *J Comput Chem* 25(13):1584-1604.
41. Phillips JC*, et al.* (2005) Scalable molecular dynamics with NAMD. *Journal of Computational Chemistry* 26(16):1781-1802.
42. Jo S, Kim T, Iyer VG, & Im W (2008) CHARMM-GUI: A web-based graphical user interface for CHARMM. *Journal of Computational Chemistry* 29(11):1859-1865.
43. Jorgensen WL, Chandrasekhar J, Madura JD, Impey RW, & Klein ML (1983) Comparison of Simple Potential Functions for Simulating Liquid Water. *Journal of Chemical Physics* 79(2):926-935.
44. Beglov D & Roux B (1994) Finite Representation of an Infinite Bulk System - Solvent Boundary Potential for Computer-Simulations. *Journal of Chemical Physics* 100(12):9050-9063.
45. Torrie GM & Valleau JP (1977) Nonphysical sampling distributions in Monte Carlo free-energy estimation: Umbrella sampling. *Journal of Computational Physics* 23(2):187-199.
46. Feller SE, Zhang Y, Pastor RW, & Brooks BR (1995) Constant pressure molecular dynamics simulation: The Langevin piston method. *The Journal of Chemical Physics* 103(11):4613-4621.
47. Nosé S (1984) A unified formulation of the constant temperature molecular dynamics methods. *The Journal of Chemical Physics* 81(1):511-519.
48. Hoover WG (1985) Canonical dynamics: Equilibrium phase-space distributions. *Physical Review A* 31(3):1695-1697.
49. Ryckaert J-P, Ciccotti G, & Berendsen HJC (1977) Numerical integration of the cartesian equations of motion of a system with constraints: molecular dynamics of n-alkanes. *Journal of Computational Physics* 23(3):327-341.
50. Darden T, York D, & Pedersen L (1993) Particle mesh Ewald: An N·log(N) method for Ewald sums in large systems. *The Journal of Chemical Physics* 98(12):10089-10092.
51. Kumar S, Rosenberg JM, Bouzida D, Swendsen RH, & Kollman PA (1992) THE weighted histogram analysis method for free-energy calculations on biomolecules. I. The method. *Journal of Computational Chemistry* 13(8):1011-1021.
52. Vorobyov I, Bennett WF, Tieleman DP, Allen TW, & Noskov S (2012) The Role of Atomic Polarization in the Thermodynamics of Chloroform Partitioning to Lipid Bilayers. *J Chem Theory Comput* 8(2):618-628.
53. Jo S, Kim T, Iyer VG, & Im W (2008) CHARMM-GUI: a web-based graphical user interface for CHARMM. *J Comput Chem* 29(11):1859-1865.

54. Lee S*, et al.* (2014) CHARMM36 united atom chain model for lipids and surfactants. *J Phys Chem B* 118(2):547-556.
55. Shaw DE*, et al.* (2014) Anton 2: Raising the bar for performance and programmability in a special-purpose molecular dynamics supercomputer. *Sc14: International Conference for High Performance Computing, Networking, Storage and Analysis*:41-53.

Appendix SA1. RosettaLigand docking scripts

```
<ROSETTASCRIPTS>
    <SCOREFXNS>
        <ligand_soft_rep weights="ligand_soft_rep">
            <Reweight scoretype="fa_elec" weight="0.42"/>
            <Reweight scoretype="hbond_bb_sc" weight="1.3"/>
            <Reweight scoretype="hbond_sc" weight="1.3"/>
            <Reweight scoretype="rama" weight="0.2"/>
        </ligand_soft_rep>

        <hard_rep weights=ligand>
            <Reweight scoretype="fa_intra_rep" weight="0.004"/>
            <Reweight scoretype="fa_elec" weight="0.42"/>
            <Reweight scoretype="hbond_bb_sc" weight="1.3"/>
            <Reweight scoretype="hbond_sc" weight="1.3"/>
            <Reweight scoretype="rama" weight="0.2"/>
        </hard_rep>
    </SCOREFXNS>

    <LIGAND_AREAS>
        <docking_sidechain chain="X" cutoff="7.0"
add_nbr_radius="true" all_atom_mode="true" minimize_ligand="10"/>
        <final_sidechain chain="X" cutoff="7.0"
add_nbr_radius="true" all_atom_mode="true"/>
        <final_backbone chain="X" cutoff="7.0"
add_nbr_radius="false" all_atom_mode="true"
Calpha_restraints="0.3"/>
    </LIGAND_AREAS>

    <INTERFACE_BUILDERS>
        <side_chain_for_docking
ligand_areas="docking_sidechain"/>
        <side_chain_for_final ligand_areas="final_sidechain"/>
        <backbone ligand_areas="final_backbone"
extension_window="3"/>
    </INTERFACE_BUILDERS>

    <MOVEMAP_BUILDERS>
        <docking sc_interface="side_chain_for_docking"
minimize_water="true"/>
        <final sc_interface="side_chain_for_final"
bb_interface="backbone" minimize_water="true"/>
    </MOVEMAP_BUILDERS>

    <SCORINGGRIDS ligand_chain="X" width="20">
        <vdw grid_type="ClassicGrid" weight="1.0"/>
    </SCORINGGRIDS>

<MOVERS>
```

```
        <Transform name="transform" chain="X" box_size="10.0"
move_distance="0.1" angle="5" cycles="1000" repeats="1"
temperature="5" initial_perturb="10.0"/>
        <HighResDocker name="high_res_docker" cycles="6"
repack_every_Nth="3" scorefxn="ligand_soft_rep"
movemap_builder="docking"/>
        <FinalMinimizer name="final" scorefxn="hard_rep"
movemap_builder="final"/>
        <InterfaceScoreCalculator name="add_scores" chains="X"
scorefxn="hard_rep" compute_grid_scores="0"
native="/home/tigerous/projects/input/EeNav-hNav1.5-open-
inactivated-lidocaine0/EeNav-hNav1.5-open-inactivated-
lidocaine0.pdb"/>
        AddJobPairData name="system_name" key="system_name"
value_type="string" value_from_ligand_chain="X"

        <ParsedProtocol name="low_res_dock">
            <Add mover_name="transform"/>
        </ParsedProtocol>

        <ParsedProtocol name="high_res_dock">
            <Add mover_name="high_res_docker"/>
            <Add mover_name="final"/>
        </ParsedProtocol>

        <ParsedProtocol name="reporting">
            <Add mover_name="add_scores"/>
            Add mover_name="system_name"
        </ParsedProtocol>
    </MOVERS>

    <PROTOCOLS>
        <Add mover_name="low_res_dock"/>
        <Add mover_name="high_res_dock"/>
        <Add mover_name="reporting"/>
    </PROTOCOLS>

</ROSETTASCRIPTS>
```

RosettaLigand docking flags

```
/home/tigerous/Rosetta_workstation/main/source/bin/rosetta_script
s.linuxgccrelease \
-in:path:database
/home/tigerous/Rosetta_workstation/main/database \
-in:file:s /home/tigerous/projects/input/EeNav-hNav1.5-open-
inactivated-refine-lidocaine0/20-
models/${SLURM_ARRAY_TASK_ID}.pdb \
```

```
-in:file:native /home/tigerous/projects/input/EeNav-hNav1.5-open-
inactivated-refine-lidocaine0/20-
models/${SLURM_ARRAY_TASK_ID}.pdb \
-parser:protocol /home/tigerous/projects/input/EeNav-hNav1.5-
open-inactivated-refine-lidocaine0/EeNav-hNav1.5-open-
inactivated-refine-lidocaine0-20ligand-10A.xml \
-nstruct 2000 \
-extra_res_fa /home/tigerous/projects/input/EeNav-hNav1.5-open-
inactivated-refine-lidocaine0/EeNav-hNav1.5-open-inactivated-
refine-lidocaine0.params \
-use_input_sc \
-packing \
-ex1 \
-ex2 \
-extrachi_cutoff 3 \
-out:prefix docking_ligand \
-out:file:silent /share/work/tigerous/work/Dock-ligand-20ligands-
200k-EeNav-hNav1.5-open-inactivated-refine-lidocaine0-
_/${SLURM_ARRAY_TASK_ID}/docking_ligand_EeNav-hNav1.5-open-
inactivated-refine-lidocaine0_${SLURM_ARRAY_TASK_ID}.silent \
-out:file:silent_struct_type binary \
-mute all
```

Appendix SA2. Charged lidocaine (LID1) optimized CHARMM force field topology and parameter files.

```
* Initial topologies generated by
* CHARMM General Force Field (CGenFF) program version 1.0.0
* For use with CGenFF version 3.0.1
36 1

! "penalty" is the highest penalty score of the associated
parameters.
! Penalties lower than 10 indicate the analogy is fair; penalties
between 10
! and 50 mean some basic validation is recommended; penalties higher
than
! 50 indicate poor analogy and mandate extensive
validation/optimization.

!=============================================================
! Lidocaine +
!=============================================================

RESI LID1       1.000
GROUP            ! CHARGE   CH_PENALTY
ATOM C1     CG331  -0.268 !    0.366
ATOM C2     CG324   0.057
ATOM N1     NG3P1  -0.264
ATOM C3     CG324   0.057
ATOM C4     CG331  -0.268 !    0.366
ATOM C5     CG324   0.493
ATOM C6     CG2O1   0.101
```

```
ATOM O1     OG2D1  -0.372 !    5.333
ATOM N2     NG2S1  -0.393
ATOM C7     CG2R61  0.021
ATOM C8     CG2R61  0.249
ATOM C9     CG2R61 -0.110 !    0.000
ATOM C10    CG2R61 -0.113 !    0.000
ATOM C11    CG2R61 -0.110 !    0.000
ATOM C12    CG2R61  0.249
ATOM C13    CG331  -0.466
ATOM C14    CG331  -0.466
ATOM H1     HGA3    0.090 !    0.060
ATOM H2     HGA3    0.090 !    0.060
ATOM H3     HGA3    0.090 !    0.060
ATOM H4     HGA2    0.090 !    0.000
ATOM H5     HGA2    0.090 !    0.000
ATOM H6     HGA2    0.090 !    0.000
ATOM H7     HGA2    0.090 !    0.000
ATOM H8     HGA3    0.090 !    0.060
ATOM H9     HGA3    0.090 !    0.060
ATOM H10    HGA3    0.090 !    0.060
ATOM H11    HGA2    0.090 !    3.750
ATOM H12    HGA2    0.090 !    3.750
ATOM H13    HGP1    0.318 !    7.260
ATOM H14    HGR61   0.115 !    0.000
ATOM H15    HGR61   0.115 !    0.000
ATOM H16    HGR61   0.115 !    0.000
ATOM H17    HGA3    0.090 !    0.000
ATOM H18    HGA3    0.090 !    0.000
ATOM H19    HGA3    0.090 !    0.000
ATOM H20    HGA3    0.090 !    0.000
ATOM H21    HGA3    0.090 !    0.000
ATOM H22    HGA3    0.090 !    0.000
ATOM H23    HGP2    0.320 !    1.252

BOND C1   C2
BOND C1   H1
BOND C1   H2
BOND C1   H3
BOND C2   N1
BOND C2   H4
BOND C2   H5
BOND N1   C3
BOND N1   C5
BOND N1   H23
BOND C3   C4
BOND C3   H6
BOND C3   H7
BOND C4   H8
BOND C4   H9
BOND C4   H10
BOND C5   C6
BOND C5   H11
BOND C5   H12
BOND C6   O1
BOND C6   N2
```

```
BOND N2   C7
BOND N2   H13
BOND C7   C12
BOND C7   C8
BOND C8   C9
BOND C8   C14
BOND C9   C10
BOND C9   H14
BOND C10  C11
BOND C10  H15
BOND C11  C12
BOND C11  H16
BOND C12  C13
BOND C13  H17
BOND C13  H18
BOND C13  H19
BOND C14  H20
BOND C14  H21
BOND C14  H22
IMPR C6     C5     N2     O1

END

BONDS

ANGLES
CG2O1  CG324  NG3P1    43.70    110.00 ! LID1 , from CG2O1 CG324
NG3P3, penalty= 1.5
CG331  CG324  NG3P1   100.00    110.00 ! LID1 , from CG321 CG324
NG3P1, penalty= 0.9

DIHEDRALS
NG2S1  CG2O1  CG324  NG3P1      0.4000  1     0.00 ! LID1 , from
NG2S1 CG2O1 CG324 NG3P3, penalty= 1.5
OG2D1  CG2O1  CG324  NG3P1      0.0000  1     0.00 ! LID1 , from
OG2D1 CG2O1 CG324 NG3P3, penalty= 1.5
CG324  CG2O1  NG2S1  CG2R61     0.7260  1     0.00
CG324  CG2O1  NG2S1  CG2R61     2.3230  2   180.00
NG3P1  CG324  CG331  HGA3        0.1600  3     0.00 ! LID1 , from
NG3P0 CG324 CG331 HGA3, penalty= 1.2
CG2O1  CG324  NG3P1  CG324      2.2550  1     0.00
CG2O1  CG324  NG3P1  CG324      1.1680  2     0.00
CG2O1  CG324  NG3P1  CG324      0.5700  3   180.00
CG2O1  CG324  NG3P1  HGP2        3.0000  3     0.00
CG331  CG324  NG3P1  CG324      0.1000  3     0.00 ! LID1 , from
CG321 CG324 NG3P1 CG324, penalty= 0.9
CG331  CG324  NG3P1  HGP2        0.1000  3     0.00 ! LID1 , from
CG321 CG324 NG3P1 HGP2, penalty= 0.9

IMPROPERS
CG2O1  CG324  NG2S1  OG2D1    120.0000  0     0.00 ! LID1 , from
CG2O1 CG321 NG2S1 OG2D1, penalty= 0.1

END
```

Neutral lidocaine (LID0) optimized CHARMM force field topology and parameter files.

```
* Initial topologies generated by
* CHARMM General Force Field (CGenFF) program version 1.0.0
* For use with CGenFF version 3.0.1
36 1

! "penalty" is the highest penalty score of the associated
parameters.
! Penalties lower than 10 indicate the analogy is fair; penalties
between 10
! and 50 mean some basic validation is recommended; penalties higher
than
! 50 indicate poor analogy and mandate extensive
validation/optimization.

!============================================================
! Lidocaine 0
!============================================================

RESI LID0         0.000
GROUP            ! CHARGE   CH_PENALTY
ATOM C1     CG331  -0.273 !    3.560
ATOM C2     CG321  -0.048 !    9.830
ATOM N1     NG301  -0.515
ATOM C3     CG321  -0.048 !    9.830
ATOM C4     CG331  -0.273 !    3.560
ATOM C5     CG321   0.310
ATOM C6     CG2O1   0.635
ATOM O1     OG2D1  -0.491 !    9.416
ATOM N2     NG2S1  -0.749
ATOM C7     CG2R61  0.477
ATOM C8     CG2R61  0.409
ATOM C9     CG2R61 -0.110 !    0.000
ATOM C10    CG2R61 -0.113 !    0.000
ATOM C11    CG2R61 -0.110 !    0.000
ATOM C12    CG2R61  0.409
ATOM C13    CG331  -0.897
ATOM C14    CG331  -0.897
ATOM H1     HGA3    0.090 !    0.030
ATOM H2     HGA3    0.090 !    0.030
ATOM H3     HGA3    0.090 !    0.030
ATOM H4     HGA2    0.090 !    3.536
ATOM H5     HGA2    0.090 !    3.536
ATOM H6     HGA2    0.090 !    3.536
ATOM H7     HGA2    0.090 !    3.536
ATOM H8     HGA3    0.090 !    0.030
ATOM H9     HGA3    0.090 !    0.030
ATOM H10    HGA3    0.090 !    0.030
ATOM H11    HGA2    0.090 !    3.536
ATOM H12    HGA2    0.090 !    3.536
ATOM H13    HGP1    0.319 !    0.000
ATOM H14    HGR61   0.115 !    0.000
ATOM H15    HGR61   0.115 !    0.000
```

```
ATOM H16    HGR61   0.115 !    0.000
ATOM H17    HGA3    0.090 !    0.000
ATOM H18    HGA3    0.090 !    0.000
ATOM H19    HGA3    0.090 !    0.000
ATOM H20    HGA3    0.090 !    0.000
ATOM H21    HGA3    0.090 !    0.000
ATOM H22    HGA3    0.090 !    0.000

BOND C1   C2
BOND C1   H1
BOND C1   H2
BOND C1   H3
BOND C2   N1
BOND C2   H4
BOND C2   H5
BOND N1   C3
BOND N1   C5
BOND C3   C4
BOND C3   H6
BOND C3   H7
BOND C4   H8
BOND C4   H9
BOND C4   H10
BOND C5   C6
BOND C5   H11
BOND C5   H12
BOND C6   O1
BOND C6   N2
BOND N2   C7
BOND N2   H13
BOND C7   C12
BOND C7   C8
BOND C8   C9
BOND C8   C14
BOND C9   C10
BOND C9   H14
BOND C10  C11
BOND C10  H15
BOND C11  C12
BOND C11  H16
BOND C12  C13
BOND C13  H17
BOND C13  H18
BOND C13  H19
BOND C14  H20
BOND C14  H21
BOND C14  H22
IMPR C6     C5     N2     O1

END

BONDS
CG321  NG301   263.00     1.4740 ! LID0 , from CG321 NG311, penalty=
5
```

```
ANGLES
CG2O1  CG321  NG301    43.70    110.00 ! LID0 , from CG2O2 CG321
NG321, penalty= 3.3
CG331  CG321  NG301    43.70    112.20 ! LID0 , from CG331 CG321
NG311, penalty= 0.6
NG301  CG321  HGA2     32.40    109.50   50.00   2.13000 ! LID0 ,
from NG311 CG321 HGA2, penalty= 0.6
CG321  NG301  CG321    52.597   92.533

DIHEDRALS
NG301  CG321  CG331  HGA3       0.1600  3     0.00 ! LID0 , from
NG311 CG321 CG331 HGA3, penalty= 0.6
NG2S1  CG2O1  CG321  NG301      0.8900  1     0.00
CG2O1  CG321  NG301  CG321      2.9130  1     0.00
CG2O1  CG321  NG301  CG321      0.6530  2     0.00
CG2O1  CG321  NG301  CG321      1.6990  3     0.00
OG2D1  CG2O1  CG321  NG301      2.5020  1     0.00
CG331  CG321  NG301  CG321      1.5370  1     0.00
CG331  CG321  NG301  CG321      0.3330  2     0.00
CG331  CG321  NG301  CG321      1.3380  3     0.00
HGA2   CG321  NG301  CG321      0.2650  3   180.00

IMPROPERS


end
```